Arabian Journal for Science and Engineering
https://doi.org/10.1007/s13369-020-04765-3

RESEARCH ARTICLE-ELECTRICAL ENGINEERING

Sudden Cardiac Arrest (SCA) Prediction Using ECG Morphological Features

M. Murugappan[1] · L. Murugesan[2] · S. Jerritta[3] · Hojjat Adeli[4]

Received: 30 January 2020 / Accepted: 1 July 2020

Abstract
Sudden cardiac arrest (SCA) prediction using electrocardiogram (ECG) and heart rate variability (HRV) signals has received the attention of researchers in recent years. Ventricular fibrillation (VF) is one of the most common identifiers for SCA. This work aims to investigate the ECG morphological feature, *R* peak to *T*-end (R–T_{end}), to foresee the imminent SCA 5 min before VF onset. ECG signals for SCA and Normal Controls from The MIT-BIH databases are divided into 1-min duration and is used to predict the onset of VF. Four nonlinear features, the Largest Lyapunov Exponent, Hurst exponent, sample entropy, and approximate entropy were extracted from the R–T_{end} beats and classified using three classifiers: support vector machine, subtractive fuzzy clustering, and neuro-fuzzy classifier. The performance of the proposed methodology confirms that the sample entropy features efficiently predict the SCA five min before VF onset using SVM classifier and produces the maximum mean classification rate of 100% compared to other classifiers. The proposed algorithm using R–T_{end} beats predicts the onset of SCA better than HRV signals and is computationally efficient. The proposed marker based on ECG morphological characteristics can be used as a tool to predict SCA for smarter healthcare management.

Keywords Electrocardiogram (ECG) · Machine learning · Nonlinear features · Sudden cardiac arrest (SCA) · Ventricular fibrillation (VF) · R–T_{end} beats · HRV signals

1 Introduction

Sudden cardiac arrest (SCA) appears primarily due to the sudden electrical disturbances in the heart, and when it stops pumping the blood to the rest of the body [1]. This unpredictable electrical activity of the heart rapidly increases the heartbeats, which is further influenced by arrhythmias and conditions such as ventricular fibrillation (VF) and ventricular tachycardia (VT) [2]. In specific, if these disturbances are not treated within a short period, generally within a few minutes, it can lead to sudden cardiac death (SCD). Recent statistics reveal that a higher mortality rate due to cardiac arrest is reported in out-of-hospital than the subjects under medication [3]. In specific, the survival rate of cardiac arrest (CA) patients out-of-hospital is less than 30%, and sudden changes in heart rate (HR) and QRS complex have been observed 1 h before CA [4]. Concurrently, they pointed out that age is one of the critical factors which significantly influences CA, and very few studies in the literature explored ECG morphological changes before in-hospital CA (IHCA). Based on the recent study, almost 84% of SCD is due to ventricular tachyarrhythmia (VTA), and the remaining 16% is due to bradyarrhythmia (BA) [5]. Timely medical care of SCA can prevent SCD, which has been identified as one of the significant cardiac issues, significantly affecting people in both developed and developing countries. Recent statistics by American Heart Association (AHA) indicate the presence of more than 600,000 fatalities each year due to cardiac diseases, and one in seven people will die of SCD

✉ M. Murugappan
m.murugappan@gmail.com; m.murugappan@kcst.edu.kw

1 Department of Electronics and Communication Engineering, Kuwait College of Science and Technology (KCST), Doha, Kuwait

2 School of Computer Engineering, Universiti Malaysia Perlis (UniMAP), Arau, Perlis, Malaysia

3 Department of Electronics and Communication Engineering, Vels Institute of Science, Technology and Advanced Studies (VISTAS), Chennai, India

4 Departments of Biomedical Informatics, Neurology, and Neuroscience, The Ohio State University, Columbus, OH 43220, USA

Published online: 26 July 2020

in the IUSA [6]. SCD is affected by risk predictors such as coronary artery diseases (CAD), valvular diseases (VD), channelopathies, myocardial infarction (MI), and genetic factors [2]. CAD is the most common factor for SCD. Still, in younger adults, arrhythmogenic right ventricular cardiomyopathy (ARVC), hypertrophic cardiomyopathy (HCM), anomalous coronary arteries, and hereditary channelopathies are the most common sources for SCD [5]. Several factors influence the condition of the heart, and an early prediction of a probable SCA can not only help in lifestyle changes but also enable an appropriate and timely medical intervention, thereby reducing the number of fatal incidents.

SCA researchers employ data from patients with heart conditions such as dilated cardiomyopathy (DCM) and coronary heart disease (CHD) for prediction. Various invasive and noninvasive risk markers such as left ventricular ejection fraction (LVEF), baroreceptor sensitivity (BRS), QT dispersion, and T wave alternans (TWA) have been used to segregate high- and low-risk SCD patients. The patients who have reduced Left Ventricular (LV) function following MI and DCM are classified as high-risk patients of SCD [7]. While patients with high-risk SCD receive prophylactic Implantable Cardio Defibrillator (ICD), it is also important to note that SCD events occur in significant numbers in low-risk patients who do not receive ICD. A review of current risk stratification methods and future risk stratification schemes to identify high-risk patients of SCA is discussed in detail in [7, 8]. Though different researchers in the literature have proposed several risk markers, all these markers are developed and tested with few numbers of samples and it lacks of generalization. Hence, these markers need extensive validation with large number of samples before its being incorporated in clinical practice as an efficient clinical risk marker. Besides, none of them is computationally efficient because the earlier works required a large number of sample ECG signals for training and consequently higher demands for computational time and memory. Hence, coming up with a prediction marker that requires a fewer number of samples and less computational time is of great interest. A review of different risk stratification methods in SCD using ECG signals is presented by Gimeno-blanes et al. [9].

ECG signals portray dynamic, nonlinear, and chaotic behavior. As such nonlinear analysis of these signals based on chaos theory [10] is used to obtain insightful information on the underlying physical conditions of the heart electrical activity. Chaos theory and fractality measures [11] have been used successfully for automated diagnosis of various neurological disorders such as epilepsy [12, 13], mild cognitive impairment (MCI) [14], the Alzheimer's disease [10, 15], autistic spectrum disorder (ASD) [16, 17], Parkinson's disease [18, 19], and depression [20] in conjunction with signal processing techniques such as wavelet transform [21, 22] and neurocomputing and machine learning [23–26]. Hence, the use of these nonlinear features could extract meaningful information about a minute changes in heart rhythm to effectively predict SCA.

Recently, morphological features from biosignals received major attention in clinical diagnosis. Segovia et al. [27] discuss diagnosis of Parkinsonism based on the striatal morphology. The morphology of the ECG waveform plays a significant role in identifying the state of the subject. The changes in electrical potential patterns (P-QRS-T) play a significant role in diagnosing cardiac health. These geometrical patterns are subtle and need a lot of clinical acumen for proper diagnosis. A recent study by Lim et al. [28], presents the significance of morphological changes in identifying the abnormalities of the ECG signal and they indicated that the minimal to significant variation in P-Wave, QRS complex and T wave results in a true positive rate of 98% to identify the abnormalities in signal. In another work, the same researchers have developed a biometric authentication system using ECG morphological features [29]. In the case of SCD, most of the earlier works in the literature discuss the ECG parameter changes within the QT interval to analyze the depolarization and repolarization in the heart. The ECG parameters, such as fragmented QRS (fQRS), QT prolongation, heart rate variability (HRV), QRS complex, T-peak to T-end (Tpe), heart rate turbulence (HRT) and T wave alternans (TWA) have predictive value for the arrhythmic events [30–33]. In [34], the researchers analyze the morphological changes within QT prolongation, such as R-wave onset to R peak, R peak to R-wave end, ST-segment duration, T wave onset to T-peak, and T-peak to T wave end with SCD. Finally, they concluded that T-peak to T-end is highly associated with SCD risk assessment. Recently, the researchers have analyzed the J-point or J-wave in the QRS complex, which exists between the QRS complex and the ST-segment has potential in analyzing the early repolarization. It may indicate the presence of VF [35, 36]. The most comprehensive review of different types of clinical risk markers in conduction, repolarization, and both stages can be found in [35]. In this case, cardiac monitoring by analyzing the ECG parameters is an effective way to determine the future occurrence of the fatal VT/VF. Several methods are used to extract information about these various conditions and abnormalities present in the ECG signal. Researchers also indicate that a computer-based methodology with nonlinear methods can capture these variations with better accuracy [37]. Recently, a software tool has been developed by a group of researchers for extracting linear, nonlinear, and time–frequency features from HRV signals for diagnosing different cardiac pathologies [38].

2 Literature Review

Sankari et al. [39] present Heart Saver, a mobile cardiac monitoring system for automatic detection of atrial fibrillation, MI, and atrio-ventricular block. Martis et al. [40] review methods used for electrocardiogram characterization. Martis et al. [41] discuss computer aided diagnosis of atrial arrhythmia using dimensionality reduction methods. A spectrum of linear and nonlinear features has been investigated for signal processing applications in both engineering and clinical domains [42]. QT interval, QRS duration, signal-averaged electrocardiogram (SAECG), and TWA measurements from ECG signals have been employed to assess the risk of SCD [43]. Juan et al. [44] worked on ECG signals using wavelet packet transform, and probabilistic neural network classifier and obtained 95.8% accuracy. They measured the Homogeneity Index to measure the uniformity or smoothness of the signal [45]. QT waves are significant, but the higher complexity involved in QT interval measurement limits its prognostic ability, as discussed in a recent study [46]. These parameters seem to do better in predicting high-risk than low-risk SCD cases. HRV features derived from ECG have been used in many studies to predict SCD and Ventricular Arrhythmias (VA). Kleiger et al. [47] found HRV signals to be useful in predicting sudden and non-sudden death of post-MI patients. While HRV has been used as an active marker to predict several conditions, recently, researchers have worked on individual impulse waveforms or a combination of impulse waveforms produced by different specialized cardiac tissues to predict and understand the various conditions of the heart.

Sun et al. [48] report the nonlinear parameter Hurst results in 100% accuracy when segregating the VT/VF episodes from normal sinus rhythm (NSR) beats. Jelinek et al. [49] found that the complex correlation measure (CCM) was inferior in patients with major depressive disorder (MDD) than normal control (NC). This inferior CCM indicated a dampening of oscillations between parasympathetic and sympathetic oscillatory activity, which indicates a reduced functionality and increased risk of SCD. Huikuri et al. [50] used a detrended fluctuation analysis feature called scaling exponent ($\alpha 1$) as a risk predictor for SCD in 446 patients with MI and LVEF $\leq 35\%$. They investigated three nonlinear features, DFA $\alpha 1$, the standard deviation of normal–normal (SDNN), and very low-frequency spectral components, to develop a powerful SCD predictor for cumulative arrhythmic and non-arrhythmic survival during 1200 days of follow-up. They concluded that DFA $\alpha 1 < 0.75$ was a useful SCD predictor among the other predictors such as standard deviation of short-term variability (SD1) and standard deviation of long-term variability (SD2) in Poincare plots. Time-dependent Point Correlation Dimension (PD2i) derived from HRV produces a maximum specificity and sensitivity of 100% and 85% in detecting VF/VT, respectively [51]. Similarly, the short-term fractal scale from heart rate indicated an increased risk of SCD in elderly subjects [52]. Five statistical features (number of ectopic beats, the standard deviation of heart rate, power at low frequency, normalized power at low frequency and total power) and two nonlinear features (standard deviation of short-term variability and fractal scaling exponent) derived from HR 5 min before the onset of an SCA achieved 96.36% accuracy [53].

Shen et al. [54] had utilized four-time domain features with Multi-Layer Perceptron (MLP) and reported 67.44% accuracy in predicting imminent SCA using 2 min of HRV. Ebrahimzadeh et al. [55] extracted 20 different types of features from 1 min of an HRV signal and produced 91.23% accuracy in predicting imminent SCA 1 min before its onset. Later, the researchers worked on extracting different features from multiple domain analyses reported prediction rates of 83.96% and 81.49% using MLP and kNN, respectively, for predicting imminent SCA 3 min before its occurrence [56]. Hamida et al. [57] used HRV signals to predict the SCD using time–frequency analysis, which is 4 min before the VF onset from the MIT/BIH database.

Recently, 5-min durations of HRV and respiration rate variability (RRV) signals were extracted from 52 SCD patients, which is 1 h before VT onset for predicting the SCD. They achieved a maximum mean classification rate of 85.3% using different time, frequency, and nonlinear domain features [58]. Reko et al.[59] used 8 h of ECG recording to study the underlying patterns for predicting imminent SCA. Mahalanobis Distance (MD) and Fitting Error Ratio (FER) measures were extracted from the recording and statistical analysis performed. A maximum mean accuracy of 78.4% in predicting imminent Sustained VTA and 73.9% accuracy for imminent non-sustained VTA were reported [59]. Skinner et al. [51] proposed a nonlinear descriptor named time-dependent point correlation dimension (PD2i) for SCA detection. Evaluation of this descriptor on 15–30 min of VT/VF HRV produced 100% sensitivity and 85% specificity.

Most of these research works are based on ECG or HRV signals and analyzed the complete or portion of ECG signal traces for defining the risk marker and to detect SCA several minutes before the VF onset. The maximum SCA prediction accuracy achieved and reported in the literature is about 96%. However, there is no research work reported in the literature on morphological feature-based SCA prediction. Understanding the significance of nonlinear and morphological features, in this research, the morphological features of the R–T_{end} beats are used to investigate the cardiac system from ventricular depolarization to ventricular repolarization and understand VT and VF conditions of the heart to predict

SCA. To the best of our knowledge, there is no conspicuous work that discusses ECG morphological features (R–T_{end}) to predict SCA using nonlinear features and machine learning algorithms is reported in the literature. Hence, this present work aims to analyze the geometrical patterns of the ECG signals and attempts to predict SCA by extracting nonlinear features from the R–T_{end} segment of the ECG.

Hence, this present work is aimed to utilize the nonlinear features extracted from ECG morphology, i.e., R–T_{end} segments of the ECG wave, to predict SCA with better accuracy. The four most significant types of nonlinear features, approximate entropy (ApEN), sample entropy (SampEN), largest lyapunov exponent (LLE) [60], and Hurst exponent (HE) were extracted from the R–T_{end} segment of ECG signals and statistically evaluated using ANOVA with a $p < 0.001$. The statistically discriminate features were classified using SVM, SFC, and NFC. Performance metrics such as mean accuracy (Acc), specificity (Spe), sensitivity (Sen), positive predictive value (PPV) and negative predictive value (NPV) are used to assess the performance of the proposed SCA prediction system. The research methodology of the proposed work and the details of experimental results and conclusions are given in the following sections.

3 Methodology

The flow diagram used in this work is as indicated in Fig. 1. The steps are elaborated as follows.

3.1 Database

Most of the earlier works in the literature on SCA prediction/detection using ECG and HRV signals utilized MIT/BIH database for SCA prediction [61]. In this work, two databases, the NSR database for non-SCA and SCD database for SCA, from MIT/BIH database, are used for the SCA prediction. Data for 18 subjects (15 males, three females) from the SCD database with age ranging from 17 to 82 years, and 18 subjects (five males, 13 females) from the NSR database with age ranging from 20 to 45 years are utilized in this work. The data was obtained directly from hospitals around Boston and were measured using Holter recording. The total number of samples per second in both databases is 256. More details about the patients, experimental setup, experimental procedure, data acquisition, patient health history, and annotation have been presented in Goldberger et al. [62].

In order to predict the SCA, ECG signals of 1-min duration at 5 min before the extraction of VF onset were segmented from all the signals in the SCD database. In the case of non-SCA, 1-min ECG segments were chosen from all the data in the NSR category.

3.2 Pre-processing

Pre-processing of a signal is an essential stage in terms of signal conditioning. It is used to remove unwanted information such as noise and artifacts from the signal. In this research, two-stage filtering was performed using an IIR filter and S-Transform to remove noise from the ECG signals, including baseline wandering, power line interference, and muscle artifacts [63]. First, the noise due to power line frequency and baseline wandering was removed by using a 6th order IIR filter with passband frequencies between 0.5 and 49 Hz. To remove the *zero-energy* noise that was present in the desired frequency range (0.5–49 Hz) of the ECG signals, Stockwell Transform (S-Transform), which is a phase-corrected Continuous Wavelet Transform (CWT) [64–67], was used in the second stage of filtering [64].

The continuous S-Transform (τ, f_o) is defined as [55],

$$S_o(\tau, f_o) = \int_{-\infty}^{\infty} \frac{x(t)|f_o|}{\sqrt{2\pi}} e^{\frac{-(\tau-t)^2 f_o^2}{2}} e^{-i2\pi f_o t} \mathrm{d}t \tag{1}$$

where $x(t)$ is the input signal, and τ is the time of spectral localization. The output of the S-transform (τ, f_o), is a one-dimensional function of time at a constant frequency

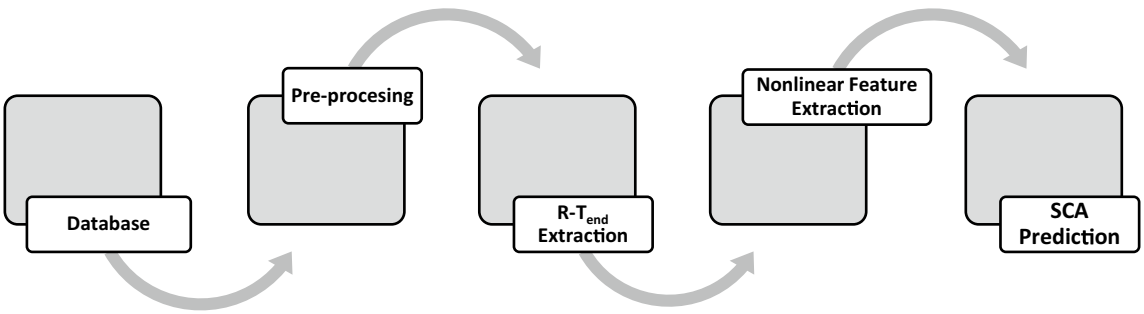

Fig. 1 Methodology on SCA prediction using ECG morphological features

f_o. Assuming that the input signal $x(t)$ is windowed using Gaussian function $g(t)$, then the output spectrum is given by

$$H(f) = \int_{-\infty}^{\infty} x(t)g(t)e^{-i2\pi ft}\mathrm{d}t \tag{2}$$

where generalized Gaussian function is ($g(t)$) is defined as

$$g(t) = \frac{1}{\sigma\sqrt{2\pi}}e^{\frac{-t^2}{2\sigma^2}} \tag{3}$$

Therefore, the continuous *S*-Transform function in Eq. (1) can be represented by Gaussian function with translation (τ) and dilation (σ) parameters as

$$S(\tau, f_o, \sigma) = \int_{-\infty}^{\infty} x(t)\frac{1}{\sigma\sqrt{2\pi}}e^{\frac{-(t-\tau)^2}{2\sigma^2}}e^{-i2\pi f_o t}\mathrm{d}t \tag{4}$$

In this work, the *S*-Transform window size (σ) in Eq. (4) was varied between 0.1 and 2.0 with an increment of 0.1 for both SCA and non-SCA filtered signals to analyze its ability to remove *zero-energy* noises from the filtered signals. The value of σ was fixed as 0.2 and 1.6 for efficient removal of *zero-energy* noises from SCA and non-SCA filtered signals, respectively, based on visual inspection.

3.3 R–T_{end} Extraction

A typical ECG signal with the PQRST complex contains three segments, namely, PR segment, QRS complex, and the ST-segment. In [68], the researchers have proposed an adaptive signal extraction method based on DWT coupled with adaptive parameters to extract different morphological waves from the highly varied ECG signals. In specific, the proposed method efficiently extracts the ECG morphological waves such as P-wave, QRS complex, T wave, and onset and offset of P-wave using adaptive parameters even if the ECG signal changes due to any cause. The proposed method achieved a maximum mean sensitivity of 95% in extracting the morphological waves from the public databases. In this work, the authors aim to investigate and analyze the ECG signal from ventricular depolarization up to the end of ventricular repolarization, which is from the *R* peak to the end of *T* wave (R–T_{end}). The other segments, such as S wave and QRS complex, are not considered, as the performance of SCA prediction can be significantly improved while analyzing the R–T_{end} segment, which is directly associated with SCA than other segments.

However, extracting differentiating features from the R–T_{end} segment is challenging due to the fluctuations in the baseline, signal characteristics, and frequency of the *T* wave. Several methods have been proposed by different researchers in the literature for *R* peak and *T* wave extraction. In this study, R peaks are detected using the R peak detection method in [47], and T_{end} was identified according to the method proposed by Zhang et al. [42].

Based on the *R* peak detected, an interval [t_1, t_2] is roughly chosen to delimit the T_{end} for each cardiac cycle. t_1 and t_2 are the starting and ending time of the *T* wave. A moving window integrator with a window size of the width, *W*, is chosen such that the $0 < W < L$, where *L* indicates the total length of the *T* wave given as.

$$L = t_2 - t_1 \tag{5}$$

The area under the *T* wave $A(t)$, is computed at every instant of time using the moving window, as in Fig. 2.

$$A(t) = \int_{t-W}^{t} [s(\tau) - s(t)]\mathrm{d}\tau \tag{6}$$

A (t) refers to the area under the signal (t) in the interval [$t-W$, t]. T_{end} (t_2) is located by finding the value of t that maximizes the area $A(t)$. In this work, the total number of R–T_{end} beats and their characteristics in one-min durations, 5 min before imminent SCA, is used for devising electrophysiological markers for SCA prediction.

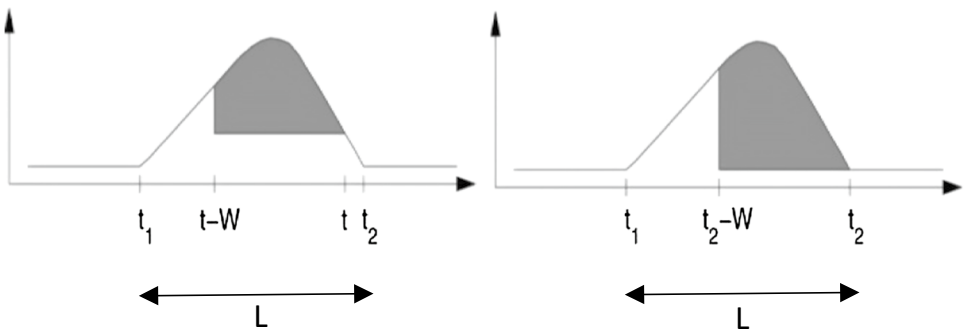

Fig. 2 Area calculation using a window of size *W*, t_1 and t_2 indicate the start and end time of *T* wave

3.4 Extraction of Nonlinear Features

The nonlinear and chaotic behavior of the ECG signals depend on the condition of the heart, and abnormal fluctuations caused due to cardiovascular diseases increase the chaotic nature of the ECG signals [69]. ECG signals pertaining to SCA and also reflects an increase in the chaotic and nonlinear behavior depending on the severity of the cardiac arrest. As such differences can be measured using nonlinear analysis, nonlinear features such as largest Lyapunov exponent (LLE), Hurst exponent (HE), entropies, etc., are explored in this work as a measure of the complexity and regularity of the time series.

3.4.1 Largest Lyapunov Exponent

Largest Lyapunov exponent (LLE) denoted by λ is given by [34],

$$\lambda(k) = \frac{1}{k\Delta t}\frac{1}{M-k}\sum_{n=1}^{M-k}\ln\frac{d_n(k)}{d_n(0)} \tag{7}$$

where Δ is the sampling period, M is the embedding dimension, $d_n(k)$ is the distance between the kth pair of nearest neighbors after k discrete-time steps. LLE measures the divergence rate of two initially nearby points of a trajectory as the system evolves. The orbits of the trajectory can be distinguished as chaotic when λ is positive and static when λ is negative. The individual information present in the R–T_{end} beats to estimate the Lyapunov exponent is called the degree of freedom, and it decides the total number LLEs. In this work, LLE was computed on the R–T_{end} beats based on algorithms devised by Rosenstein et al. [70].

3.4.2 Approximate Entropy

Approximate entropy (ApEN) measures similar epochs in a given time series data. Time series with highly repetitive patterns have small values of ApEN, and those with less predictable patterns have a higher value of ApEN [46]. Thus, ApEN is an effective measure to quantify unpredictability of fluctuation in R–T_{end} beats that is more specific in SCA [71].

$$\begin{aligned}\text{ApEN}(d,R,L) = {} & \frac{1}{N-d+1}\sum_{i=1}^{L-d+1}\log C_i^d(R) \\ & -\frac{1}{L-d}\sum_{i=1}^{L-d+1}\log C_i^{d+1}(R)\end{aligned} \tag{8}$$

where the correlation integral,

$$C_i^d = \frac{1}{L-d+1}\sum_{i,j=1}^{L-d+1}\Phi(R-\|x_i-x_j\|) \tag{9}$$

and d denotes embedding dimension, R indicates the similarity criterion, L refers to the data length, and Φ is the step function. In this work, the value of d is 2, R is 20% of the standard deviation of the time-series segment.

3.4.3 Sample Entropy

Sample Entropy (SampEN) is a measure similar to approximate entropy that quantifies the level of complexity that exists in the signal [61]. Higher values of SampEN denote lower regularity in time series and vice versa.

$$s(d,R,L) = -\ln[\phi'^d(R)/\phi'^{d+1}(R)] \tag{10}$$

where,

$$\phi'^m(R) = (L-d+1)\int_{i=1}^{L-d+1}A_i'(R) \tag{11}$$

is the correlation integral. The embedding dimension and the similarity criterion values are chosen to be the same as ApEN. Recent studies have indicated both SampEN and ApEN can be useful tools in understanding the dynamics of the physiology of cardiovascular systems, and hence both are used in the present work [61].

3.4.4 Hurst Exponent

Hurst exponent (HE) is used to measure the smoothness of fractal time series data. The computation of HE is based on the asymptotic behavior of the rescaled range of the underlying process [71, 72]

$$HE = \log\left(\frac{R'}{S}\right)/\log(L) \tag{12}$$

where L is the length of the data, $'$ is the difference between the maximum and minimum deviation from the mean value, and S refers to the standard deviation of the time series data.

The values of HE ranges from 0 to 1 and is a measure of the roughness of the time series. Higher values of HE, ranging from 0.5 to 1, indicate the existence of a strong correlation in the data. Values less than 0.5 indicate anti-persistent or a rougher time series. HE values of 0.5 indicates a Brownian motion or random data that cannot be predicted.

3.5 Prediction of SCA

Three classifiers, namely Subtractive Fuzzy Clustering (SFC) [56], Support Vector Machine (SVM) [57], and Neuro-Fuzzy Classifier (NFC) [58] are used to predict SCA. The nonlinear features extracted from individual R–T_{end} beats are used to identify the underlying dynamic state.

3.5.1 Subtractive Fuzzy Classifier

SFC generally requires lesser computational time than the Fuzzy C Means (FCM) clustering. Consider a collection of m data point $\{ x_1, \ldots, x_m \}$ in an N-dimensional space. Subtractive Fuzzy Classifier (SFC) assumes each data point is a potential cluster center and calculates a measure of the potential for each data point based on the density of surrounding data points. Density measure at data point x_j is calculated as,

$$D_j = \sum_{i=1}^{m} \exp\left(-\frac{\left| x_j - x_i \right|^2}{(r_a/2)^2} \right) \tag{13}$$

where r_a is a positive constant, and it defined as the neighborhood radius.

SFC algorithm selects the data point with the highest density measure as the first cluster center and then destroys the potential of data points near the first cluster center. The range of influence of a cluster center in each data dimension is called a cluster radius. A small cluster radius (radii parameter) will lead to finding many small clusters in the data (resulting in many fuzzy rules) and vice versa. In this work, the radii parameter was experimented from 0.1 to 1.0 with an increment of 0.1. If the performance of the SFC algorithm is improving when the radii equals to 1.0, then the radii parameter would be further incremented in binary expansion (2^n, n=1,2,3,…,128) until the prediction accuracy begins to drop.

3.5.2 Support Vector Machine

Support Vector Machine (SVM) is a robust, binary classification algorithm that employs sophisticated mathematical principles to provide better classification based on statistical learning theory. It uses a hyperplane to segregate the two classes depending on the kernel used. Let the separating hyperplane to be defined as $x \cdot w + b = 0$, where w is the weight vector, x is the input vector, and b is the bias. For linearly separable data labeled $\{x_i, y_i\}, x_i \in \Re^N d, y_i = \{-1, 1\}, i = 1, \ldots, N$, the optimum boundary chosen with maximal margin criterion is found by minimizing the objective function,

$$E = \|w\|^2$$

Subject to $(x_i \cdot w + b)y_i \geq 1$, for all i. The solution for the optimal boundary w_0 is a linear combination of a subset of training data, $s \in \{1, \ldots, N\}$: the support vectors. These support vectors define the margin edges and satisfy equality $(x_s \cdot w_0 + b)y_s = 1$. Data may be classified by computing the sign of $x \cdot w_0 + b$.

3.5.3 Neuro-Fuzzy Classifier

Neuro-Fuzzy classifier (NFC) works on the principle of Neural Networks (NN) and the Fuzzy Inference System (FIS) [54, 55]. FIS addresses problems that are not linearly separable by employing knowledge from human experts in the form of IF–THEN rules [73]. NFC is fundamentally an algorithm with the learning ability of NN and represents learned knowledge in an interpretable using FIS [17, 74]. There are many types of NFCs reported in the literature and this work utilizes the NFC with scaled conjugate gradient (SCG) algorithm [71]. It combines the compelling description of FIS with the learning capability of NN to partition a feature space into classes. NFCs have been applied to various problems and situations. It consists of 6 layers (input, fuzzy membership, fuzzification, defuzzification, normalization and output) and can handle problems with multiple inputs and multiple outputs [74]. The use of weights in the defuzzification layer affects the rules and improves classification flexibility. In this work, k-means clustering method is used to obtain the initial parameters and to formulate the fuzzy IF–THEN rules [75]. This reduces the complexity associated with its implementation.

3.6 Performance Metrics

The performance of different classifiers for SCA prediction is evaluated using five performance metrics: mean accuracy (Acc), sensitivity (Sen), specificity (Spe), positive predictive value (PPV), and negative predictive value (NPV) as defined by Eqs. (14)–(18) [53].

$$\text{Acc} = \frac{\text{TP} + \text{TN}}{\text{TP} + \text{TN} + \text{FP} + \text{FN}} \tag{14}$$

$$\text{Sen} = \frac{\text{TP}}{\text{TP} + \text{FN}} \tag{15}$$

$$\text{Spe} = \frac{\text{TN}}{\text{TN} + \text{FP}} \tag{16}$$

$$\text{PPV} = \frac{\text{TP}}{\text{TP} + \text{FP}} \tag{17}$$

$$\mathrm{NPV} = \frac{\mathrm{TN}}{\mathrm{TN} + \mathrm{FN}} \tag{18}$$

where TP, TN, FP, and FN refer to the total number of true positive, true negative, false positive, and false-negative samples, respectively.

4 Numerical Results

The noise in the ECG signal was removed using Butterworth IIR and S-Transform-based filtering methods. The 6th order IIR Butterworth band-pass filter with a frequency ranging

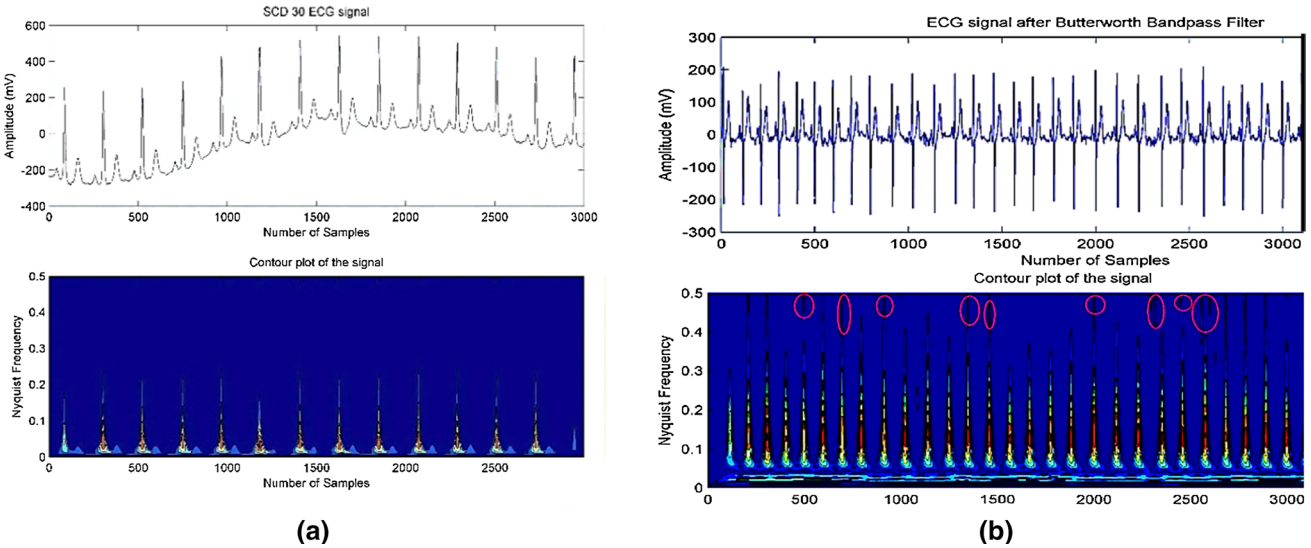

Fig. 3 **a** Raw ECG signal of SCD patient no 30 with contour plot. **b** Band-pass filtered signal of ECG signal of SCD patient no 30 with a contour plot

Fig. 4 S-transform filtered signal of EEG signal of SCD patient no 30 with a contour plot

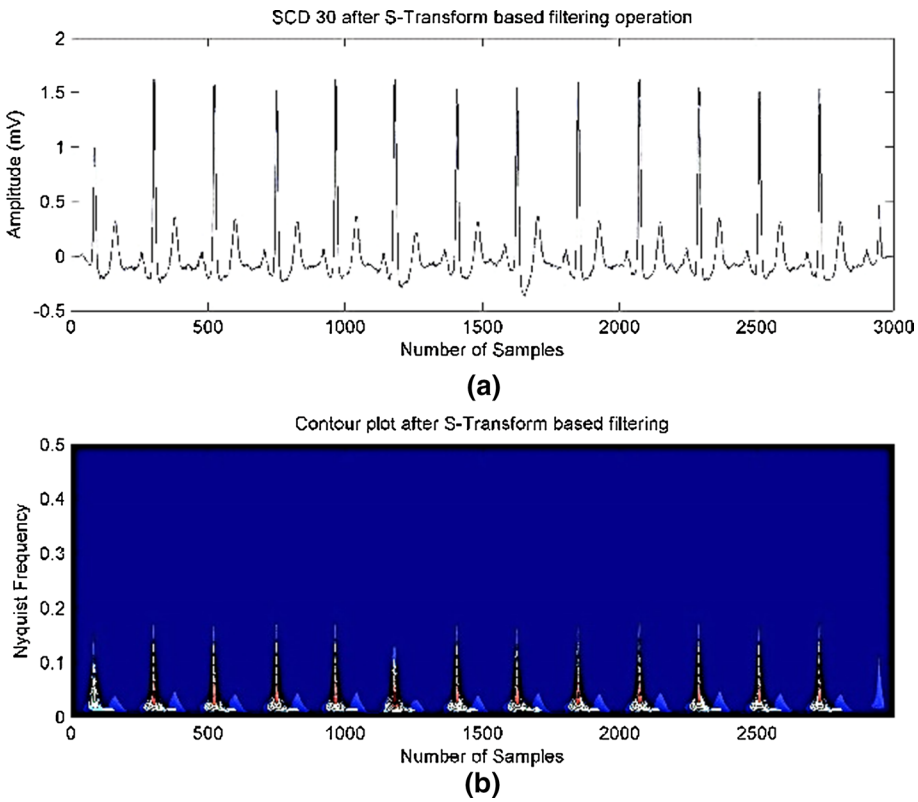

from 0.5 to 49 Hz removed baseline wandering, power line interference, and high-frequency noise from the SCA and non-SCA signals.

Figure 3a displays a sample ECG signal for an SCD patient on the top and its contour plot at the bottom representing the normalized frequency of the signal. The sample indicates the presence of baseline wandering and which was removed using Butterworth filter. The filtered signal and its contour are represented in Fig. 3b. The red-colored circles in Fig. 3b indicate the presence of noises at higher frequencies, which needs to be removed for accurate prediction of SCA. Noises with *zero energy* appear as black lines on the contour plot. In this research, an S-transform filter is employed to remove the *zero-energy* noise. The filtered output is shown in Fig. 4. Initially, the ECG signals are normalized using the average mean reference method to transform the signal amplitude between − 1 to 1, and then S-Transform is applied to the normalized signal to remove the *zero energy* noises.

4.1 Statistical Analysis

The four nonlinear features were obtained from the R–T_{end} beats of the 36 ECG records (18 SCD records and 18 normal ECG records). The number of R–T_{end} beats varied in the range of 82–96 beats per minute for both NSR and SCD signals. In this work, 82 R–T_{end} beats were extracted from both SCD and NSR signals and used for feature extraction. The dimension of the feature vector of each feature derived from a single R–T_{end} beat over 36 EEG records was $[2952 \times 1]$. The box plot analysis of features values of NSR and SCD is shown in Fig. 5. The two subjects group have notable differences in their feature values between normal control and SCD. These variations are significant due to the changes in the geometry of the waveform, indicating the divergence of the values is different for both the cases. The values derived from RR variability and others do not show signs as the R–T_{end} beats.

Table 1 Statistical analysis of R–T_{end} beats features using one-way ANOVA

Nonlinear features	One-way ANOVA	
	F value	p value
LLE	363.57	$6.5e^{-8}$
ApEN	178.98	$7.8e^{-10}$
SampEN	108.11	$9.2e^{-9}$
HE	779.20	$5.3e^{-12}$

In this work, ANOVA is used for testing the statistical significance of all the features indicating a significant difference in the values between the two states. The results are listed in Table 1. The high F values, all greater than 100, and the shallow p values, all less than 0.0001, indicating that all the nonlinear features were statistically significant in demarcating the SCA and non-SCA data. HE has the least value of p, followed by ApEn, SampEN, and LLE, indicating

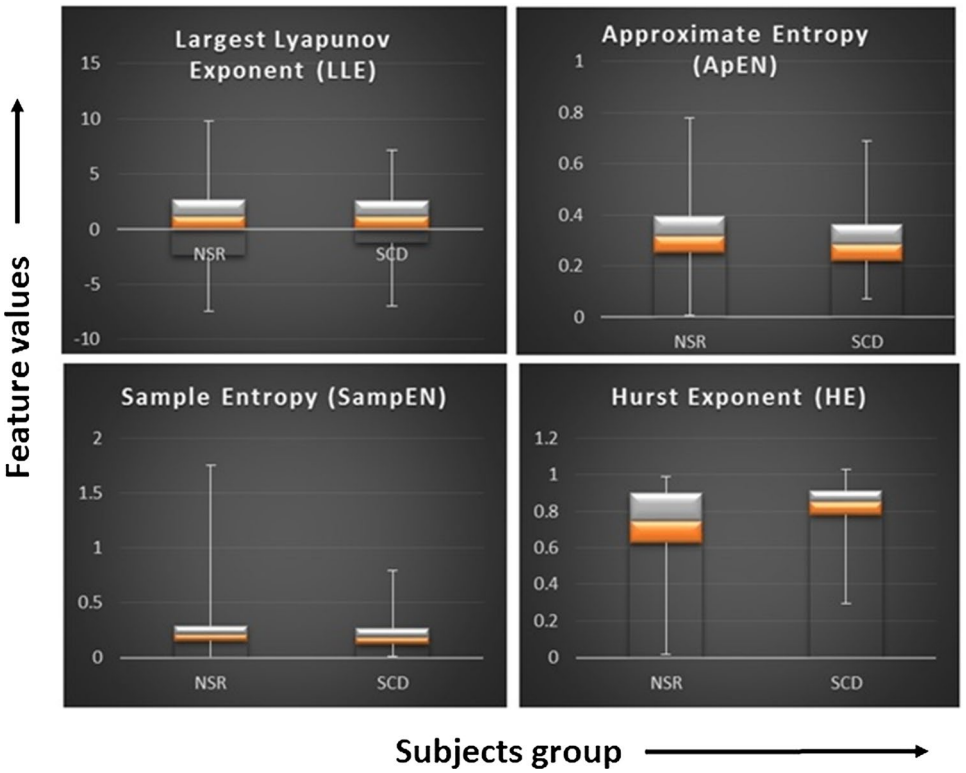

Fig. 5 Box plot analysis of largest Lyapunov exponent (LLE) (top left), approximate entropy (ApEN) (top right), sample entropy (SampEN) (bottom left), and Hurst exponent (HE) (bottom right)

Table 2 SCA prediction rate using support vector machine classifier (%)

Features	SPE	SEN	PPV	NPV	Acc
ApEN	100	97.22	100	97.56	98.68
SampEN	100	100	100	100	100
HE	100	88.89	100	90.91	94.74
LLE	100	94.44	100	95.24	97.37

Spe specificity, *Sen* sensitivity, *PPV* positive predictive value, *NPV* negative predictive value, *Acc* mean accuracy

Table 3 SCA prediction rate using subtractive fuzzy classifier (%)

Features	Spe	Sen	PPV	NPV	Acc
ApEN	100	83.33	100	86.96	92.11
SampEN	100	97.22	100	97.56	98.68
HE	90	75	87.10	80	82.89
LLE	75	97.22	77.78	96.77	85.53

Spe specificity, *Sen* sensitivity, *PPV* positive predictive value, *NPV* negative predictive value, *Acc* mean accuracy

Table 4 SCA prediction rate using neuro-fuzzy classifier (%)

Features	Spe	Sen	PPV	NPV	Acc
ApEN	95	97.22	94.59	97.44	96.05
SampEN	95	100	94.74	100	97.37
HE	87.5	72.22	83.87	77.78	80.26
LLE	90	80.56	87.88	83.72	85.33

the order of significance, which was further explored using the classifiers.

4.2 Prediction of SCA Using the Various Classifiers

Before employing machine learning algorithms for SCA classification, the *k*-fold cross-validation method was used to segregate all the features into training and testing sets. The value of 10 was used for *k* to perform random division of the features into 10 (*k*) equal data sets. Of these nine sets (− 1) were used for training, and the *k*th set used for testing. The accuracy of the classifiers was cross-validated by repeating the process for 10 (*k*) times by changing the sets used for training and testing.

The mean classification values over the ten trials are reported in this section. The performances of the three classifiers using four different features are presented in Tables 2, 3 and 4. It can be observed from Table 2 that for SVM, all the features predict SCA with an accuracy of at least 94%, and the entropy feature, namely Approximate Entropy

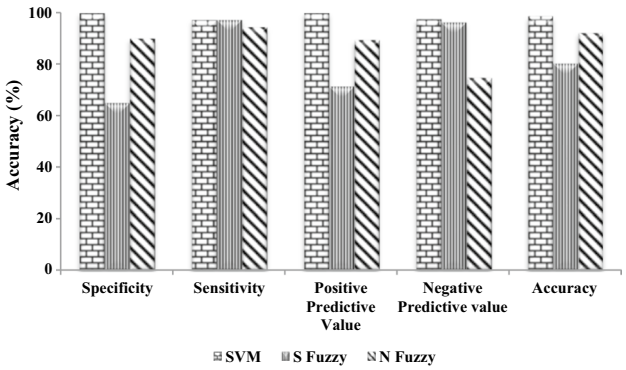

Fig. 6 Comparison of performance metrics

and Sample Entropy, yields the highest accuracy in the range 98.7–100%. This same trend is observed in the SFC (Table 3) and NFC (Table 4), where the entropy features outperform the other features.

Overall, Sample Entropy was able to differentiate SCA from non-SCA most effectively with an accuracy of 100%, 98.68%, and 97.37% for SVM, SFC, and NFC, respectively. The sensitivity, specificity, PPV, and NPV of the Sample Entropy feature were also high compared to the other features in the analysis, indicating that the SCA and non-SCA cases are predicted correctly in most cases.

The performance metrics of all the features and three classifiers are summarized in the bar chart of Fig. 6. The linear kernel used in the SVM classifier indicates that the features of SCA and non-SCA data were linearly separable. Indeed, the SVM classifier has more parameters to be fine-tuned than the other two classifiers (*C*: regularization parameter, *gamma*: kernel coefficient, type of kernel function) [76]. NFC and SFC, on the other hand, are more suitable for feature vectors with a nonlinear pattern, thus explaining their lower mean accuracies. The maximum accuracy for all the features by combining all the four features is 98.68%, 80.26%, and 92.11% for SVM, Subtractive Fuzzy, and Neuro-Fuzzy classifiers, respectively. SFC gives the lowest mean classification rate compared to other classifiers, because, the average mean values of HE features of NSR and SCD features have a smaller range of values than LLE and Sample Entropy. Alongside, LLE gives maximum mean classification rate than HE features, since, the LLE values of NSR features are higher than SCD features, which could imply that the data was more chaotic for SCD cases (Table 3). It should be noted that all the features have excellent negative predictive value (more than 80%) and higher sensitivity (more than 83%). In specific, entropy measures are efficient in capturing the dynamics of R–T_{end} beats relevant to VF/VT onset compared to LLE and Hurst exponents. These experimental results confirmed the findings of earlier work on

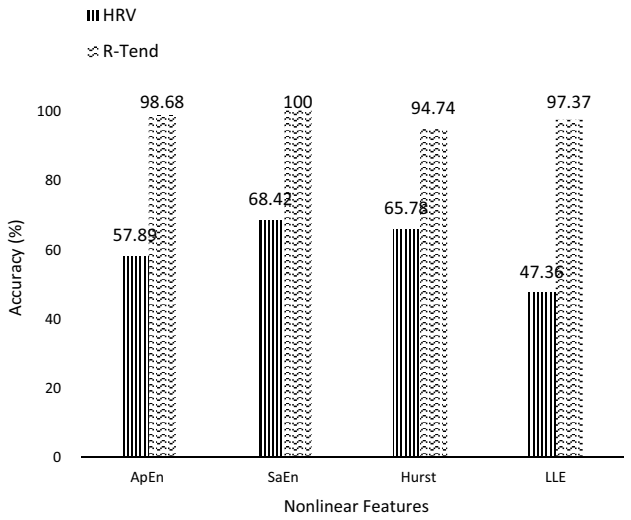

Fig. 7 Comparison of accuracy of SCA prediction using HRV versus R–T_{end} signals using SVM

nonlinear features-based SCA prediction using ECG signal in [56].

The performance of the R–T_{end} beats was also compared with HRV signals for all the four nonlinear features. The results for SVM are shown in Fig. 7. It can be observed that all the nonlinear features performed better for the R–T_{end} beats compared to that of HRV signals using the SVM classifier. This analysis indicates that R–T_{end} can be investigated further using a large number of signals to predict the onset of SCA

5 Discussion

5.1 Significance of ECG Morphology

Researchers working on the prediction of various heart diseases typically investigate ECG and HRV signals to develop intelligent healthcare systems. Devising eminent risk markers can allow the system to identify the pathology in a computationally efficient way. Several risk stratification methods have been proposed in the literature for identifying the risk of SCD using different markers Left Ventricular Ejection Fraction (LVEF), Heart rate turbulence (HRT), deceleration capacity, and microvolt T wave alternans (MTWA), etc.

While these methods are suitable for predicting the SCA from a healthy heart, they are inefficient in real-time and under other medical conditions such as VF/VT and have stacks of challenges in computation. Most of the existing prediction algorithms in the literature report substandard sensitivity or specificity or negative predictive value and most successful in predicting SCD in patients with cardiac diseases. Most of the earlier works analyzed HRV signals for predicting SCA before the onset of VF/VT, other waveforms produced by the cardiac system such as QRS and ST should also be analyzed in accordance with its significance to the underlying conditions.

Several studies have been published for predicting SCA/SCD using different waves or segments from patient's ECG, such as the QRS duration, QT prolongation, ST elevation, ST depression, TWA, QT dispersion, and heart rate variability. More details about the different types of risk markers in SCA predication can be found in [9]. R–T_{end} waves reflecting the ventricular depolarization and repolarization behavior have been researched extensively to understand their correlation with the occurrence of SCA. Results indicate that R–T_{end} waves are significant in predicting the onset of SCA and can be investigated further to be developed as an efficient marker for SCA prediction clinically. Besides the R–T_{end} features, the other morphological features also have a significant difference between normal control and SCD. QT prolongation of normal control and SCD has a mean value of 0.404 s (Ranges: 0.401–0.407 s), 0.414 s (ranges: 0.407–0.416 s), respectively. In case of T-peak to T-end duration, the normal control and SCD has a mean value of 0.0764 s (0.0737–0.0778 s), 0.0884 s (0.0867–0.0922 s), respectively. The QRS duration of SCD (>0.138 s) is greater than normal control (>0.10 s).

5.2 Nonlinear Features from Varied Morphology of ECG Signals

Both linear and nonlinear features are analyzed by researchers for the prediction and identification of SCA. It is well evident that nonlinear features perform well compared to linear features in SCA prediction in both ECG and HRV signals [46, 48, 51, 56, 58].

A selected number of computationally efficient nonlinear features were used in this work to extract the hidden underlying patterns that correlate with SCA. These nonlinear features produce highly significant results for 5 min of imminent SCA prediction as compared with earlier works in the literature (Table 5). Understanding the significance of morphology and nonlinear features, the present study computed nonlinear features from the R–T_{end} wave of the ECG signals and reported high accuracy. Table 5 provides a comparison of the results from the current study with earlier works on SCA prediction using ECG and HRV signals. The MIT/BIH databases (SCD and NSR) was used in most of the works as an international standard database for SCA/SCD detection. In [58], the HRV signals are used to predict the SCA 4 min before VF onset and achieved a maximum prediction rate of 94.7% compared to other researchers. Fairooz et al. [77] achieved a maximum SCA prediction rate of 91.67% in predicting the SCA 30 min before its onset with a maximum mean accuracy of 91.67%. Besides, most of the research work analyzed multiple domains (time, frequency,

Table 5 Comparison of present work with earlier works in SCA prediction in %

References	Duration of signal	Sen	Spe	Acc
Shen et al. [54]	2 min of HRV right up to onset of VF(SCA)	–	–	67.44
Ebrahimzadeh et al. [55]	1 min of HRV which is 1 min before the onset of VF (SCA)	–	–	91.23
Ebrahimzadeh et al. [56]	1 min of HRV which is 3 min before the onset of VF (SCA)	83.75	0.159	83.93
	1 min of HRV which is 2 min before the onset of VF (SCA)	89.64	0.089	90.36
Hamido et al. [58]	1 min HRV which is 4 min before VF onset	95	94.40	94.7
Lee et al. [57]	60 min ECG before VTA	88.2	82.4	85.3
Reko et al. [59]	8 h ECG recording of sustained VTA patients	50	93	78.4
	8 h ECG recording of non-sustained VTA patients	11	93	73.9
Murukesan et al. [53]	5 min of HRV which is 2 min before the onset of VF	93.33	100.00	96.36
Skinner et al. [51]	HRV of 15–30 min for detection	100	85	–
Fairooz et al. [76]	1 min ECG which is 30 min before onset	88.88	94.44	91.67
Present work	1 min of R–T_{end} beat which is 5 min before the onset of VF (SCA)			
	SampEn	100	100	100
	ApEN	97.22	100.00	98.68
	LLE	100	95	97.37

VF ventricular fibrillation, *MLP* multi-layer perceptron, *CHF* chronic heart failure, *RRV* respiration rate variability

time–frequency) features for predicting SCA than simple features which effectively characterize the VF onset in ECG signals.

5.3 Computational Complexity and Performance

Among the different conditions of the heart, SCD/SCA is more critical as it causes fatality in a significantly short interval of time without raising any warning symptoms. The risk factor increases for patients with medical conditions. The people who suffered from VA and left ventricular (LV) systolic dysfunction over a prolonged duration of time are the prime victims of SCD. Implantable cardioverter-defibrillator (ICDs) are mostly used to save patients with a high risk of SCD. However, it is highly challenging to categorize the subjects with a significant risk of arrhythmia and to get support from ICD to rescue them from SCD.

A faster and computationally efficient algorithm is essential for efficiently predicting SCA before VF onset to reduce the mortality rate. Most of the earlier researches have computationally complex research methodology which encompasses multiple feature extraction and feature selection methods, and machine learning methods for SCA prediction. Besides, the unpredictable and complex nature of the nonlinear, non-Gaussian, and non-stationary ECG signals need to be analyzed by efficient algorithms. Hence, this research work mainly focuses on predicting the onset of VF using R–T_{end} wave information is a computationally efficient method, and it achieves a higher prediction rate compared to all other works in the literature. The complete methodology has been implemented using MATLAB software using Intel i5 processor (5th generation) with 8 GB RAM in Windows 10 operating system.

5.4 Limitations of the Present Work

The present work has the following limitations: (1) the proposed algorithm for SCA prediction is tested using a limited number of ECG samples (NSR and SCD) from the international standard MIT-BIH database. There is no open-source database for testing the proposed algorithm in clinical applications and to develop a generalized and robust SCA prediction system. (2) There is no rich information about the background of ECG data (such as patient health history, behavioral characteristics of NSR and SCD subjects, intraventricular conduction time (H–V intervals, data acquisition time, data acquisition environment, and others) is available in the database for more detail investigation of experimental results. The circadian rhythms might also significantly alter the characteristics of R–T_{end} features, and it may lead to incorrect predictions. Hence, the proposed methodology should be investigated further, taking into account the aforementioned factors to develop more robust ECG morphological feature-based risk markers for better SCA prediction.

6 Conclusion

In this work, a novel methodology is proposed for imminent SCA prediction using nonlinear features of R–T_{end} segments of ECG signals. The maximum mean classification rate of 100%, mean sensitivity of 97.12%, and a mean specificity of 97.12% have been achieved using the SVM classifier. The

SampEN feature produced a 100% mean prediction accuracy on SCA prediction. Specifically, entropy-based features are more capable of capturing randomness or chaos in a time series, and this is more evident in this present study on SCA prediction. SVM classifier fits well with the R–T_{end} features and correctly separates the SCA and non-SCA features compared to NFC and SFC classifiers. The experimental results reveal that R–T_{end} segments of the ECG signal contain useful information, which can be used for SCA prediction with perfect accuracy. This proposed algorithm could help cardiologists and medical personnel to identify and categorize high- and low-risk patients for SCA treatment or ICD implantation. Besides that, it can help to save thousands of lives in ICU wards, since medical personnel can be alerted to provide Cardiopulmonary Resuscitation (CPR) before the onset of SCA. In fact, the survival rate of SCA patients reduces by 7 to 10% with every minute of delay for CPR or defibrillation. Thus, by predicting 5 min before the onset, it is hoped that thousands of lives can be saved. However, this present work utilizes smaller size data set for developing the SCA prediction algorithm. Hence, it should be tested with a more extensive database for analyzing the generalization ability of the proposed algorithm for SCA prediction. Besides, the R–T_{end} wave the future research may focus on other ECG signal segments/waves for improved clinical interpretation/results.

Additionally, some other types of nonlinear features and advanced machine learning algorithms (such as deep learning) could further improve sudden cardiac arrest prediction system's ability in the future. The predictive power using R–T_{end} beats has been tested only on limited data and specific to the medical conditions. However, analysis over a large number of randomized trials is needed to ensure R–T_{end} beats as a computationally efficient SCD risk marker that can reduce the occurrence of Sudden Cardiac Deaths.

Compliance with Ethical Standards

Conflict of interest The authors declare that they have no conflict of interest.

Human and Animals Rights This article does not contain any studies with human participants or animals performed by any of the authors.

References

1. Zipes, D.P.; Wellens, H.J.J.: Clinical Cardiology : New Frontiers Sudden Cardiac Death, pp. 2334–2351 (2013). https://doi.org/10.1161/01.cir.98.21.2334
2. de Luna, A.B.; Coumel, P.; Leclercq, F.: Ambulatory sudden cardiac death: mechanisms of production of fatal arrhythmia on the basis of data from 157 cases. Am. Heart J. **117**, 151–159 (1989)
3. Lellouche, N.; Sacher, F.; Jorrot, P.; Cariou, A.; Spaulding, C.; et al.: Sudden cardiac arrest: ECG repolarization after resuscitation. J. Cardiovasc. Electrophysiol. **22**(2), 131–136 (2011)
4. Attin, M.; Feld, G.; Lemus, H.; et al.: Electrocardiogram characteristics prior to in-hospital cardiac arrest. J. Clin. Monit. Comput. **29**, 385–392 (2015). https://doi.org/10.1007/s10877-014-9616-0
5. Huikuri, V.; Mäkikallio, T.H.; Raatikainen, M.J.P.; Perkiömäki, J.; Castellanos, A.; Myerburg, R.J.: Prediction of sudden cardiac death: appraisal of the studies and methods assessing the risk of sudden arrhythmic death. Circulation **108**, 110–115 (2003). https://doi.org/10.1161/01.CIR.0000077519.18416.43
6. Porumb, M.; Iadanza, E.; Massaro, S.; Pecchia, L.: A convolutional neural network approach to detect congestive heart failure. Biomed. Signal Process. Control **55**, 101597 (2020). https://doi.org/10.1016/j.bspc.2019.101597
7. Liew, R.: Sudden cardiac death risk stratification. Eur. Cardiol. Rev. **10**(2), 118–122 (2015). https://doi.org/10.15420/ecr.2015.10.2.118
8. Sinner, M.F.; Rizas, K.D.; Kaab, S.: Keep it simple: the ECG and sudden cardiac death risk. Heart (2019). https://doi.org/10.1136/heartjnl-2019-316163
9. Gimeno-blanes, F.J.; Blanco-velasco, M.; Barquero-pérez, Ó.: Sudden cardiac risk stratification with electrocardiographic indices: a review on computational processing. Technol. Transf. Sci. Evid. Front. Physiol. **7**, 1–17 (2016). https://doi.org/10.3389/fphys.2016.00082
10. Adeli, H.; Ghosh-Dastidar, S.: Automated EEG-Based Diagnosis of Neurological Disorders: Inventing the Future of Neurology (2017)
11. Ortiz, A.; Munilla, J.; Martínez-Murcia, F.J.; Górriz, J.M.; Ramírez, J.: Empirical functional PCA for 3D image feature extraction through fractal sampling. Int. J. Neural Syst. **29**, 1–22 (2019). https://doi.org/10.1142/S0129065718500405
12. Ghosh-Dastidar, S.; Adeli, H.; Dadmehr, N.: Mixed-band wavelet-chaos-neural network methodology for epilepsy and epileptic seizure detection. IEEE Trans. Biomed. Eng. **54**, 1545–1551 (2007). https://doi.org/10.1109/TBME.2007.891945
13. Jiang, S.; Luo, C.; Gong, J.; Peng, R.; Ma, S.; et al.: Aberrant thalamocortical connectivity in juvenile myoclonic epilepsy. Int. J. Neural Syst. **28**(1), 1750034 (2018)
14. Fang, C.; Li, C.; Cabrerizo, M.; Barreto, A.; Andrian, J.; et al.: Gaussian discriminant analysis-based dual high-dimensional decision spaces for the diagnosis of mild cognitive impairment in Alzheimer's Disease. Int. J. Neural Syst. **28**(8), 1850017 (2018)
15. Collazos-Huertas, D.; Cardenas-Pena, D.; Castellanos-Dominguez, G.: Instance-based representation using multiple kernel learning for predicting conversion to Alzheimer disease. Int. J. Neural Syst. **29**(2), 1850042 (2019)
16. Ahmadlou, M.; Adeli, H.; Adeli, A.: Fractality and a wavelet-chaos-neural network methodology for EEG-based diagnosis of autistic spectrum disorder. J. Clin. Neurophysiol. **27**(5), 328–333 (2010)
17. Bhat, S.; Acharya, U.R.; Adeli, H.; Bairy, G.M.; Adeli, A.: Automated diagnosis of autism: in search of a mathematical marker. Rev. Neurosci. **25**(6), 851–861 (2014). https://doi.org/10.1515/revneuro-2014-0036
18. Yuvaraj, R.; Murugappan, M.; Acharya, U.R.; Adeli, H.; Ibrahim, N.M.; Mesquita, E.: Brain functional connectivity patterns for emotional state classification in Parkinson's disease patients without dementia. Behav. Brain Res. **298**, 248–260 (2016). https://doi.org/10.1016/j.bbr.2015.10.036
19. Manzanera, M.O.; Meles, S.K.; Leenders, K.L.; et al.: Scaled subprofile modeling and convolutional neural networks for the identification of Parkinson's disease in 3D nuclear imaging data. Int. J. Neural Syst. **29**(9), 1950010 (2019)

20. Acharya, U.R.; Sudarshan, V.K.; Adeli, H.; Santhosh, J.; Koh, J.E.W.; Adeli, A.: Computer-aided diagnosis of depression using EEG signals. Eur. Neurol. **73**, 329–336 (2015). https://doi.org/10.1159/000381950
21. Abbasi, A.; Bennet, L.; Gunn, A.J.; Unsworth, C.P.: Latent phase detection of hypoxic-ischemic spike transients in the EEG of preterm fetal sheep using reverse biorthogonal wavelets and fuzzy classifier. Int. J. Neural Syst. (2019). https://doi.org/10.1142/s0129065719500138
22. Wang, S.H.; Zhang, Y.D.; Yang, M.; Liu, B.; Ramirez, J.; Gorriz, J.M.: Unilateral sensorineural hearing loss identification based on double-density dual-tree complex wavelet transform and multinomial logistic regression. Integr. Comput. Aided Eng. **26**, 411–426 (2019)
23. Li, Y.; Cui, W.; Luo, M.; Li, K.; Wang, L.: Epileptic seizure detection based on time-frequency images of EEG signals using gaussian mixture model and gray level co-occurrence matrix features. Int. J. Neural Syst. **28**, 1850003 (2018). https://doi.org/10.1142/S012906571850003X
24. Sun, C.; Cui, H.; Zhou, W.; Nie, W.; Wang, X.; Yuan, Q.: Epileptic seizure detection with EEG textural features and imbalanced classification based on easy ensemble learning. Int. J. Neural Syst. (2019). https://doi.org/10.1142/s0129065719500217
25. Gorriz, J.M.; Ramirez, J.; Segovia, F.; et al.: A machine learning approach to reveal the neuro-phenotypes of autisms. Int. J. Neural Syst. **29**, 1850058 (2019)
26. Yang, T.; Cappelle, C.; Ruichek, Y.; El Bagdouri, M.: Multi-object tracking with discriminant correlation filter based deep learning tracker. Integr. Comput. Aided Eng. **26**(3), 273–284 (2019)
27. Segovia, F.; Ramirez, J.M.; Martinez-Murcia, J.; Castillo-Barnes, F.J.D.: Assisted diagnosis of Parkinsonism based on the striatal morphology. Int. J. Neural Syst. **29**(9), 1950011 (2019)
28. Lim, C.L.P.; Woo, W.L.; Dlay, S.S.; Wu, D.; Gao, B.: Deep multi-view heartwave authentication. IEEE Trans. Ind. Inform. (2018). https://doi.org/10.1109/TII.2018.2874477
29. Lim, C.L.; Woo, W.L.; Dlay, S.S.; Gao, B.: Heartrate-dependent heartwave biometric identification with thresholding-based GMM–HMM methodology. IEEE Trans. Ind. Inform. **15**(1), 45–53 (2018)
30. Abdelghani, S.A.; Rosenthal, T.M.; Morin, D.P.: Surface electrocardiogram predictors of sudden cardiac arrest. Och. J. **16**, 280–289 (2016)
31. Panikkath, R.; Reinier, K.; Evanado, A.U.; Teodorecu, C.; et al.: Prolonged T_{peak} to tend interval on the resting electrocardiogram is associated with increased risk of sudden cardiac death. Circ. Arrhythm Electrophysiol. **4**(4), 441–447 (2011). https://doi.org/10.1161/circep.110.960658
32. Mandala, S.; Di, T.C.: ECG parameters for malignant ventricular arrhythmias: a comprehensive review. J. Med. Biol. Eng. **37**, 441–453 (2017). https://doi.org/10.1007/s40846-017-0281-x
33. Tse, G.; Yan, B.P.: Traditional and novel electrocardiographic conduction and repolarization markers of sudden cardiac death. Europace **19**, 712–721 (2017). https://doi.org/10.1093/europace/euw280
34. O'Neal, W.T.; Singleton, M.J.; Roberts, J.D.; Tereshchenko, L.G.; et al.: Association between QT-interval components and sudden cardiac death the ARIC study (atherosclerosis risk in communities). Circ. Arrhythm. Electrophysiol. **10**, e005485 (2017). https://doi.org/10.1161/CIRCEP.117.005485
35. Kim, S.H.; Kim, D.Y.; Kim, H.-J.; Jung, S.M.; Han, S.W.; et al.: Early repolarization with horizontal ST segment may be associated with aborted sudden cardiac arrest: a retrospective case control study. BMC Cardiovasc. Disorders **12**, 122 (2012)
36. Haïssaguerre, M.; Nademanee, K.; Hocini, M.; Cheniti, G.; et al.: Depolarization versus repolarization abnormality underlying inferolateral J wave syndromes—new concepts in sudden cardiac death with apparently normal hearts. Heart Rhythm (2018). https://doi.org/10.1016/j.hrthm.2018.10.040
37. Huikuri, H.V.; Acharya, U.R.; Adeli, H.; Prasad, H.; et al.: Computer aided diagnosis of atrial arrhythmia using dimensionality reduction methods on transform domain representation. Biomed. Signal Process. Control **14**(17), 295–305 (2014)
38. Georgieva-Tsaneva, G.: Application of mathematical methods for analysis of digital ECG data. Inf. Technol. Control **14**(2), 35–44 (2016)
39. Sankari, Z.; Adeli, H.: HeartSaver: a mobile cardiac monitoring system for auto-detection of atrial fibrillation, myocardial infarction and atrio-ventricular block. Comput. Bio Med. **41**(4), 211–220 (2011)
40. Martis, R.J.; Acharya, U.R.; Adeli, H.: Current methods in electrocardiogram characterization. Comput. Bio Med. **48**, 133–149 (2014)
41. Martis, R.J.; Acharya, U.R.; Adeli, H.; et al.: Computer aided diagnosis of atrial arrhythmia using dimensionality reduction methods on transform domain representation. Biomed. Signal Process. Control **13**, 295–305 (2014)
42. Zhang, Q.; Manriquez, A.I.; Médigue, C.; Papelier, Y.; Sorine, M.: An algorithm for robust and efficient location of T wave ends in electrocardiograms. IEEE Trans. Biomed. Eng. **53**, 2544–2552 (2006)
43. Sudhir, S.; Brady, W.J.: Electrocardiographic differential diagnosis of st segment depression. ECG Prehospital Emerg. Care (2012). https://doi.org/10.1002/9781118473740.ch27
44. Jiang, X.; Adeli, H.: Wavelet packet-autocorrelation function method for traffic flow pattern analysis. Comput. Aid. Civ. Inf. Eng. **19**(5), 324–337 (2004)
45. Amezquita-Sanchez, J.P.; Valtierra-Rodriguez, M.; Adeli, H.; Perez-Ramirez, C.A.: A novel wavelet transform-homogeneity model for sudden cardiac death prediction using ECG signals. J. Med. Syst. **42**(10), 176 (2018). https://doi.org/10.1007/s10916-018-1031-5
46. Ho, K.K.L.; Moody, G.B.; Peng, C.-K.K.; Mietus, J.E.; Larson, M.G.; Levy, D.; Goldberger, A.L.: Predicting survival in heart failure case and control subjects by use of fully automated methods for deriving nonlinear and conventional indices of heart rate dynamics. Circulation **96**, 842–848 (1997)
47. Kleiger, R.E.; Miller, J.P.; Bigger, J.T.; Moss, A.J.: Decreased heart rate variability and its association with increased mortality after acute myocardial infarction. Am. J. Cardiol. **59**, 256–262 (1987)
48. Sun, Y.; Chan, K.L.; Krishnan, S.M.: Life-threatening ventricular arrhythmia recognition by nonlinear descriptor. Biomed. Eng. **11**, 1–11 (2005). https://doi.org/10.1186/1475-925X-4-6
49. Jelinek, H.F.; Khandoker, A.H.; Quintana, D.S.; Imam, H.; Kemp, A.H.: Complex correlation measure as a sensitive indicator of risk for sudden cardiac death in patients with depression methods and materials poincaré plot analysis. In: Conference in Computing in Cardiology, pp. 809–812 (2011)
50. Huikuri, H.V.; Ma, T.H.; Peng, C.; Goldberger, A.L.: Fractal correlation properties of R-R interval dynamics and mortality in patients with depressed left ventricular function after an acute myocardial infarction. Circulation **101**, 47–53 (2000)
51. Skinner, J.E.; Weiss, D.N.: Nonlinear analysis of the heartbeats in public patient ECGs using an automated PD2i algorithm for risk stratification of arrhythmic death. Ther. Clin. Manag. **4**, 549–557 (2008)
52. Mäkikallio, T.H.; Huikuri, H.V.; Mäkikallio, A.; Sourander, L.B.; Mitrani, R.D.; Castellanos, A.; Myerburg, R.J.: Prediction of sudden cardiac death by fractal analysis of heart rate variability in

elderly subjects. J. Am. Coll. Cardiol. **37**(5), 1395–1402 (2001). https://doi.org/10.1016/S0735-1097(01)01171-8
53. Murukesan, L.; Murugappan, M.; Iqbal, M.; Saravanan, K.: Machine learning approach for sudden cardiac arrest prediction based on optimal heart rate variability features. J. Med. Imaging Health Inform. **4**, 521–532 (2014). https://doi.org/10.1166/jmihi.2014.1287
54. Shen, T.W.; Shen, H.P.; Lin, C.H.; Ou, Y.L.: Detection and prediction of sudden cardiac death (SCD) for personal healthcare. In: 2007 29th Annual International Conference of the IEEE Engineering in Medicine and Biology Society, pp. 2575–2578 (2007). https://doi.org/10.1109/iembs.2007.4352855
55. Ebrahimzadeh, M.: Pooyan, Early detection of sudden cardiac death by using classical linear techniques and time-frequency methods on electrocardiogram signals. J. Biomed. Sci. Eng. **04**, 699–706 (2011). https://doi.org/10.4236/jbise.2011.411087
56. Ebrahimzadeh, E.; Pooyan, M.; Bijar, A.: A novel approach to predict sudden cardiac death (SCD) using nonlinear and time-frequency analyses from HRV signals. PLoS ONE **9**, 1–14 (2014). https://doi.org/10.1371/journal.pone.0081896
57. Lee, H.; Shin, S.Y.; Seo, M.; Nam, G.B.; Joo, S.: Prediction of ventricular tachycardia one hour before occurrence using artificial neural networks. Sci. Rep. **6**, 1–7 (2016). https://doi.org/10.1038/srep32390
58. Fujita, H.; Acharya, U.R.; Sudarshan, V.K.; Ghista, D.N.; Sree, S.V.; Eugene, L.W.J.; Koh, J.E.W.: Sudden cardiac death (SCD) prediction based on nonlinear heart rate variability features and SCD index. Appl. Soft Comput. J. **43**, 510–519 (2016). https://doi.org/10.1016/j.asoc.2016.02.049
59. Kemppainen, R.: ECG parameters in short-term prediction of ventricular arrhythmias (2012)
60. Spyridon, P.; Boutalis, Y.S.: Lyapunov theory based fusion neural networks for the identification of dynamic nonlinear systems. Int. J. Neural Syst. **29**(9), 1950015 (2019)
61. Moorman, J.R.: Physiological time-series analysis using approximate entropy and sample entropy. Am. J. Physiol. Heart Circ. Physiol. **2018**, 2039–2049 (2018)
62. Goldberger, A.L.; Amaral, L.A.N.; Glass, L.; Hausdorff, J.M.; Ivanov, P.C.; Mark, R.G.; Mietus, J.E.; Moody, G.B.; Peng, C.; Stanley, H.E.: PhysioBank, PhysioToolkit, and PhysioNet components of a new research resource for complex physiologic signals. Circulation **101**, E215–E220 (2000)
63. Jerritta, S.; Murugappan, M.; Wan, K.; Yaacob, S.: Emotion detection from QRS complex of ECG signals using hurst exponent for different age groups. In: Proceedings of 2013 Humaine Association Conference on Affective Computing. Intelligence Interaction ACII 2013, pp. 849–854 (2013). https://doi.org/10.1109/acii-.2013.159
64. Yuan, Q.; Zhou, W.; Xu, F.; Leng, Y.; Wei, D.: Epileptic EEG identification via LBP operators on wavelet coefficients. Int. J. Neural Syst. **28**, 1850010 (2018). https://doi.org/10.1142/S0129065718500107
65. Mishra, A.K.S.; Sahu, S.S.: ECG signal denoising using time-frequency based filtering approach. In: International Conference on Communication and Signal Processing, pp. 503–507 (2016). https://doi.org/10.1109/iccsp.2016.7754188
66. Chang, Z.; De Luca, F.; Goda, K.: Automated classification of near-fault acceleration pulses using wavelet packets. Comput. Aided Civ. Infrastruct. Eng. **34**, 569–585 (2019). https://doi.org/10.1111/mice.12437
67. Moukadem, A.; Dieterlen, N.H.; Brandt, C.: A robust heart sounds segmentation module based on S-transform. Biomed. Signal Process. Control **8**, 273–281 (2013). https://doi.org/10.1016/j.bspc.2012.11.008
68. Lim, C.L.P.; Woo, W.L.; Dlay, S.S.: Enhanced wavelet transformation for feature extraction in highly variated ECG signal. In: Proceedings of 2nd IET International Conference on Intelligent Signal Processing, 1–2 Dec, London, UK, pp. 1–6 (2015)
69. Jiang, X.; Adeli, H.: Fuzzy clustering approach for accurate embedding dimension identification in chaotic time series. Integr. Comput. Aided Eng. **10**, 287–302 (2003)
70. Rosenstein, M.T.; Collins, J.J.; De Luca, C.J.: A practical method for calculating largest Lyapunov from small data sets. Physica D **65**, 117–134 (1993)
71. Pincus, S.M.: Approximate entropy as a measure of system complexity. Proc. Natl. Acad. Sci. USA **88**, 2297–2301 (1991)
72. Cetis, Speeding up the scaled conjugate gradient algorithm and its application in neuro-fuzzy classifier training, pp. 365–378 (2010). https://doi.org/10.1007/s00500-009-0410-8.
73. Hojjat, J.: Xiaomo, Neuro-fuzzy logic model for freeway work zone capacity estimation. J. Transp. Eng. **129**, 484–493 (2003). https://doi.org/10.1061/(ASCE)0733-947X(2003)129:5(484)
74. Xu, P.; Yin, L.; Yue, Z.; Zhou, T.: On predictability of time series. Phys. A **523**, 345–351 (2019)
75. Jang, J.S.R.; Sun, C.T.; Mizutani, E.: Neuro-fuzzy and soft computing—a computational approach to learning and machine intelligence. IEEE Trans. Autom. Contin. **42**(10), 1482–1484 (1997)
76. Zhang, M.X.; Gao, L.; Chu, S.: Probability and interval hybrid reliability analysis based on adaptive local approximation of projection outlines using support vector machine. Comput. Aided Civ. Infrastruct. Eng. **34**, 991–1009 (2019). https://doi.org/10.1111/mice.12480
77. Fairooz, T.; Khammari, H.: SVM classification of CWT signal features for predicting sudden cardiac death. Biomed. Phys. Eng. Express. (2016). https://doi.org/10.1088/2057-1976/2/2/025006